PHOTONICS Research

Surface-illuminated photon-trapping high-speed Ge-on-Si photodiodes with improved efficiency up to 1700 nm

Hilal Cansizoglu,[1,†] Cesar Bartolo-Perez,[1,†] Yang Gao,[1,*] Ekaterina Ponizovskaya Devine,[1,2] Soroush Ghandiparsi,[1] Kazim G. Polat,[1] Hasina H. Mamtaz,[1] Toshishige Yamada,[2,3] Aly F. Elrefaie,[1,2] Shih-Yuan Wang,[2] and M. Saif Islam[1,4]

[1]Electrical and Computer Engineering, University of California—Davis, Davis, California 95618, USA
[2]W&WSens Devices, Inc., 4546 El Camino, Suite 215, Los Altos, California 94022, USA
[3]Electrical Engineering, Baskin School of Engineering, University of California, Santa Cruz, California 95064, USA
[4]e-mail: sislam@ucdavis.edu
*Corresponding author: yangao@ucdavis.edu

Received 20 March 2018; revised 26 April 2018; accepted 9 May 2018; posted 9 May 2018 (Doc. ID 326327); published 21 June 2018

In this paper, high-speed surface-illuminated Ge-on-Si pin photodiodes with improved efficiency are demonstrated. With photon-trapping microhole features, the external quantum efficiency (EQE) of the Ge-on-Si pin diode is >80% at 1300 nm and 73% at 1550 nm with an intrinsic Ge layer of only 2 μm thickness, showing much improvement compared to one without microholes. More than threefold EQE improvement is also observed at longer wavelengths beyond 1550 nm. These results make the microhole-enabled Ge-on-Si photodiodes promising to cover both the existing C and L bands, as well as a new data transmission window (1620–1700 nm), which can be used to enhance the capacity of conventional standard single-mode fiber cables. These photodiodes have potential for many applications, such as inter-/intra-datacenters, passive optical networks, metro and long-haul dense wavelength division multiplexing systems, eye-safe lidar systems, and quantum communications. The CMOS and BiCMOS monolithic integration compatibility of this work is also attractive for Ge CMOS, near-infrared sensing, and communication integration.

OCIS codes: (230.5170) Photodiodes; (320.7080) Ultrafast devices.

https://doi.org/10.1364/PRJ.6.000734

1. INTRODUCTION

Timely development of cost-effective and power-efficient optical interconnects is necessary to meet the high demand of data transfer in the era of the Internet of Things (IoT) that is expected to connect billions of sensors with different functionalities [1,2]. Datacenters are envisioned to scale up to meet the high demand of connectivity. Intra- and inter-datacenter communications require optical links for reach gap (500 m–2 km), long-reach (~10 km), and extended reach communications (up to 40 km), which need optical transceivers operating at wavelengths of 1300 nm (IEEE 802.3bm and IEEE 802.3bs). At the same time, passive optical networks (PONs), which provide low-cost solutions for the demand in high data rate access to users, require optical transceivers operating at a wavelength of 1550 nm [3]. The data rate can be increased in such systems by utilizing dense wavelength division multiplexing (DWDM). However, the demand for data traffic is increasing beyond the current capacity of single-mode fiber operating at the C band (1530–1560 nm) and the L band (1560–1620 nm) for DWDM in long-haul communication links. One of the promising solutions to overcome the capacity crunch is to extend existing single-mode fiber bandwidth beyond the L band. Achievements for fiber amplifiers [4,5] that can operate in the new band of 1620–1700 nm pave the way to realize data transmission beyond the L band. The new development of hollow-core photonic-bandgap fibers [6,7] has also provided a new option to extend fiber bandwidth up to 2000 nm with the use of these new optical amplifiers.

In addition, applications such as quantum communications [8], eye-safe lidar systems [9], and photonic biosensors [10], require detectors operated at the near-infrared, particularly at 1310 or 1550 nm, taking advantage of the low-loss windows of optical fibers and low scattering of light at those wavelengths in the atmosphere and tissue, respectively.

Commercially available optical receivers often contain photodiodes (PDs) based on III–V materials such as InGaAs/InP

[11,12]. However, these materials are not compatible with CMOS technology and would incur additional costs for wafer bonding, packaging, yield, thermal management, etc. [13,14]. On the other hand, monolithic integration of PDs with all electronics on a single chip, fully hermetic and without ceramic multichip carriers for the receiver end, can reduce the cost dramatically. Ge/Si devices provide a possible solution for these kinds of high-speed applications, as BiCMOS SiGe technology has already been proved in CMOS foundries [15]. In addition, low field transport is much faster in Ge than in Si, and high field transport is similar between both materials. Thus, using Ge for the i-layer in a pin PD is highly advantageous in improving speed [16].

Although bulk Ge has a very broad absorption spectrum, the direct bandgap of Ge is only 0.8 eV, which results in weak absorption at and beyond 1500 nm. However, the absorption coefficient of Ge can be greatly enhanced beyond 1500 nm by introducing tensile strain in the epitaxial Ge film on an Si substrate due to the different coefficients of thermal expansion (CTEs) [17,18]. Recent developments of Ge epitaxy on Si substrate [19], including Si_xGe_{1-x} buffer layer growth [20,21], two-step Ge growth [22,23], and selective-area growth [24], have successfully minimized the high threading dislocation densities (TDDs) caused by the 4.2% lattice mismatch between Ge and Si [25]. These TDDs can be detrimental for Ge PD applications as they reduce carrier mobility and also produce large dark current, and they must be suppressed in order to meet the economic yield standard of the device in very-large-scale integration (VLSI) or ultra-large-scale integration (ULSI) production [26].

Among the surface-illuminated photodiodes, resonant cavity enhanced (RCE) Ge PDs can exhibit both high external quantum efficiency (EQE) and high speed [27], but they are also wavelength specific and sensitive to temperature, which makes them unfavorable for optical receivers, particularly in WDM applications. Waveguide-type Ge PDs have long optical length and a short carrier collection route, so they can realize high EQE and high speed at the same time. However, due to the narrow width of the waveguide, they need tight fiber alignment, which can add additional cost [14]. On the other hand, a conventional surface-illuminated pin PD is limited by the EQE and bandwidth product as there is often a trade-off: smaller absorption thickness leads to a fast but low efficiency device, while larger absorption thickness results in an efficient but slow device. As light travels vertically into the PDs, the EQE is determined by the thickness of the absorption region (intrinsic Ge) where photons get absorbed [shown in Fig. 1(a)], and the speed of the PD also depends on the same thickness, as the transit time of the photo-generated carriers is determined by the absorption region. Our recent work has shown that this trade-off can be broken by incorporation of photon-trapping holes into Si surfaces [28,29]. As illustrated in Fig. 1(b), the photon-trapping holes can guide light nearly perpendicular to the surface and allow light to propagate laterally and eventually get absorbed through the device layer. Since the lateral dimension of the device is much larger than the thickness of the absorption layer, PDs with micro/nanoholes are efficient and fast at the same time. In addition, the micro/nanohole-based

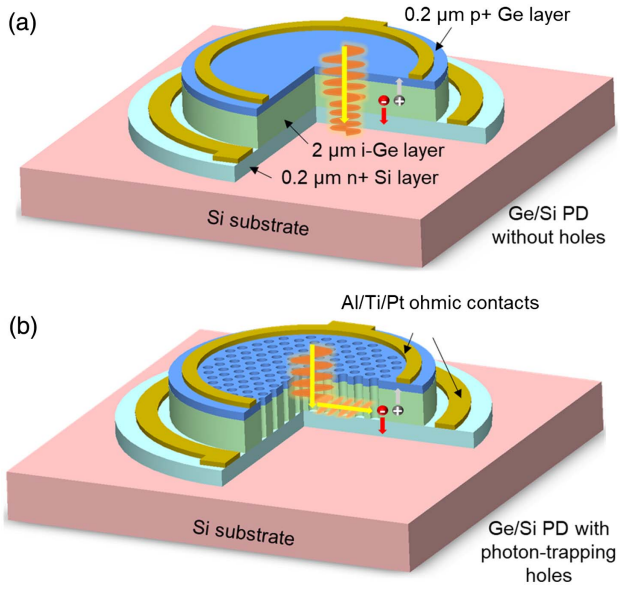

Fig. 1. Schematics of Ge/Si PD active layers (a) without holes and (b) with photon-trapping holes. The Ge-on-Si PD is composed of 0.2 μm p+Ge (blue), 2 μm i-Ge (green), and 0.2 μm n+Si (silver) layers. The yellow rings are the Al/Ti/Pt ohmic contacts. The red circle with the "−" sign and the dark circle with the "+" sign represent photon-generated electron and hole, respectively.

PD is insensitive to angular variation of the incident photons [28]. Compared to waveguide-type PDs with the limitation to a 1D array, surface-illuminated PDs can have high-density 2D arrays suitable for high data rate bandwidth communication and high spatial resolution for lidar application. In this work, we demonstrate a surface-illuminated Ge-on-Si pin PD with high EQE (>80% at 1300 nm and 73% at 1550 nm) for 10 Gb/s operation for long-haul data communication links. The EQEs of PDs with holes are enhanced to >350% up to 1700 nm compared to the PDs without holes, which is promising to realize optical receivers for data transmission beyond the L band.

2. LIGHT GUIDING WITH HOLE ARRAYS

Indirect bandgap semiconductors such as Si and Ge require a relatively thick material along the propagation direction of the incident light for effective absorption of wavelengths that have energies close to the bandgap edge of the semiconductor. The required thickness is usually of the order of the inverse value of the absorption coefficient ($1/\alpha_{\text{bulk}}$) of the semiconductor to provide a sufficient optical path for light to be fully absorbed, as shown in Fig. 2(a). For example, ~12 μm thick Ge is required for full absorption at 1550 nm wavelength, but the bandwidth of a surface-illuminated Ge pin PD with such thickness would be limited to 2 GHz. Although the strained Ge film (i.e., Ge-on-Si or Ge-on-SOI film) can improve the absorption coefficient at a longer wavelength (i.e., 1550 nm) to some extent, it is still not sufficient to overcome this speed limitation, and most importantly excessive stress in the film can cause large wafer bow, film defects, etc., ultimately causing difficulties for device fabrication and performance.

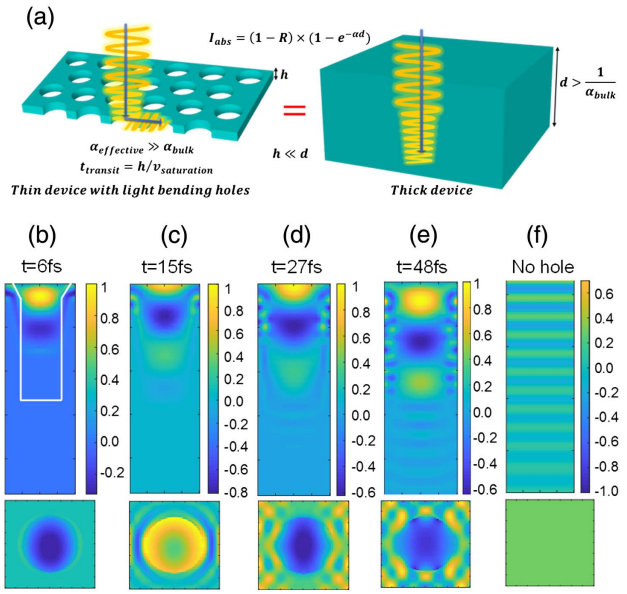

Fig. 2. (a) Schematic diagram that shows the enhanced optical path in a slab with hole arrays by light guiding near-perpendicular to the incoming light compared to an optical path in a bulk semiconductor in the direction of incident light. The effective absorption coefficient of a slab with hole arrays becomes much larger than the bulk absorption coefficient of the semiconductor due to the enhanced optical path. A thin slab with hole arrays can be used in a fast photodiode without losing efficiency, whereas a thick bulk semiconductor causes the photodiode to operate at slow speed in order to work efficiently. Typical field distributions around microholes at (b) $t = 6$ fs, (c) $t = 15$ fs, (d) $t = 27$ fs, and (e) $t = 48$ fs, showing light propagation in the lateral direction inside the material. FDTD simulations were performed for hexagonally packed tapered holes with diameter/period of 1150/1750 nm at 1550 nm wavelength for a 1.1 μm depletion layer (to be consistent with fabricated PDs demonstrated in Section 4.B). The top and bottom rows show cross sections and top views of the electric field. The border of a hole with a taper at the top is represented by white lines. (f) Simulated electric field intensity of light at 1550 nm wavelength, propagating from air into a Ge-on-Si slab without hole arrays at $t = 48$ fs. There is no sign of lateral light propagation, and light is propagating in the direction of incidence throughout the film with less intensity due to a higher surface reflection.

On the other hand, a semiconductor slab with periodic hole arrays, as shown in Fig. 2(a), can manipulate light propagation by guiding light nearly perpendicular to the incident direction. This phenomenon helps enhance the optical path in the lateral direction while allowing a relatively thin absorber material. At the Si or Ge bandgap edge, an effective absorption coefficient of the slab with photon-trapping hole arrays can be much higher than its counterpart without the holes. Such a design with hole arrays can be used to break the trade-off between the efficiency and the bandwidth of pin diodes built with indirect bandgap materials for ultra-fast communication applications.

As incident light illuminates the structure, guided modes are formed due to periodic arrays of holes [30]. Such modes have propagation constants in both the vertical and lateral directions. These guided modes trap light in the high refractive index Ge material between the air and silicon and enhance the reflection of light at the Si/Ge interface. In addition to light trapping, the hole arrays also reduce the surface reflection by reducing the refractive index difference between air and the Ge surface. Periodic holes with tapered sidewall angles can introduce a graded refractive index profile, which allows light to enter the structure smoothly.

In this study, we used the finite-difference time-domain (FDTD) method to simulate light propagation in our device structures. A periodic boundary condition was used in the directions parallel to the PD's surface, while the boundary in the direction of incident light (perpendicular to the PD's surface) was assumed to be a perfectly matched layer (PML). A set of Lorentz models was used to simulate wavelength-dependent absorption [31]. The model based on the Green's function formalism [32] was utilized in FDTD simulations for strained Ge film on Si substrate.

Light propagation in a structure with periodic hole arrays can be different from that in a slab without holes. Constructive and destructive interference of light in the incident direction is expected as light travels through a thin slab. However, a structure with periodic hole arrays interacts with light in a way that a lateral component of light propagation occurs in addition to the vertical component of propagation in the incidence direction. Figures 2(b)–2(e) show the electric field intensity of propagating light from air into the Ge-on-Si slab with periodic hole arrays calculated at particular times ($t = 6$, 15, 27, and 48 fs) at the wavelength of 1550 nm. The point of Fig. 2 is to show that hole arrays cause lateral propagation of incoming light. The top row represents the simulated electric field in the cross section of the Ge-on-Si slab with a tapered hole, and the bottom row shows the top view of the lateral propagation. By comparing Figs. 2(b)–2(e), it can be seen that light travels not only vertically but also propagates in the lateral direction in the Ge layer. Such light guiding in the thin Ge layer enhances the optical path and ultimately improves absorption without increasing thickness. Figure 2(f) shows the field propagation in Ge without holes at $t = 48$ fs (steady state; time is enough for the wave front to reach the bottom and reflect from the interface of Ge and Si) as a comparison. The light in the slab without holes propagates only in the vertical direction, and the field intensity is also smaller compared to that in the one with hole arrays due to higher reflection from the surface of the slab.

Figure 3 shows the enhancement in the absorption of Ge-on-Si PDs with hexagonally packed tapered holes (diameter/period: 1150/1750 nm), modeled numerically by using the FDTD method for a wavelength range of 1200–1800 nm. The simulated structures have a 2 μm i-layer, as shown in Fig. 1. The red and black lines in Fig. 3(a) show the simulation for the absorption of PDs with and without holes assuming that the strain in the Ge film is about 0.2% [measured from X-ray diffraction (XRD), as will be discussed in Section 4.A]. Figure 3(a) also includes the case without any strain in the Ge film for a comparison. The effect of strain on the absorption properties of the Ge films was studied in Ref. [33] and the tensile-strain effect can induce an indirect-to-direct bandgap transition and reduce the bandgap energy of Ge. Hence, strained

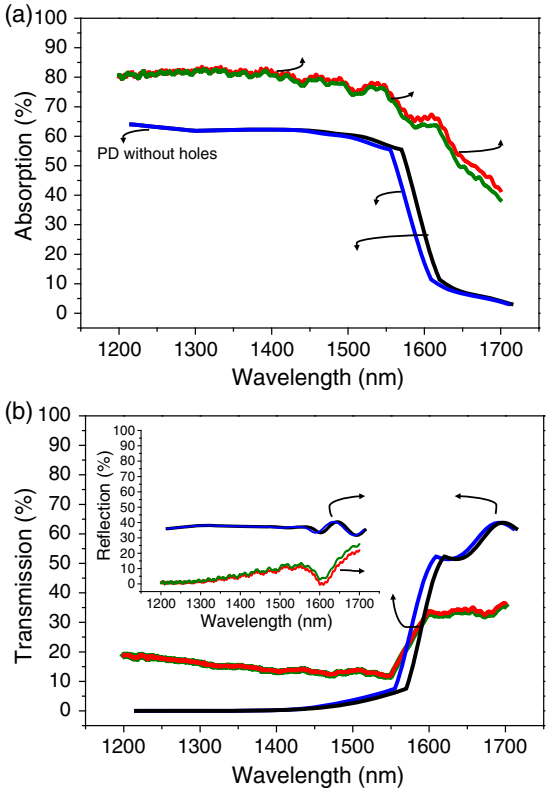

Fig. 3. (a) Calculated absorption of Ge-on-Si PDs with (red line) and without (black line) tapered holes (diameter/period: 1150/1750 nm) arranged in a hexagonal lattice for a wavelength range of 1200–1800 nm. A 0.2% strain in the Ge layer is considered during calculations. The simulated structures have a 2 μm i-layer as shown in Fig. 1. While Ge-on-Si PDs without holes theoretically absorb until 1550 nm, PDs with holes potentially keep high absorption of light up to 1700 nm. The green and blue lines represent absorption of PDs with and without holes, respectively, in the case of relaxed Ge layer as a comparison. 0.2% strain does not cause a significant difference for PDs with holes, whereas there is some improvement in absorption of PDs without holes toward longer wavelengths when a 0.2% strain is introduced to the Ge layer. (b) The calculated transmission and reflection (inset) for PDs with (red lines) and without (black lines) holes. The green and blue lines represent the case of a relaxed Ge layer as a comparison.

Ge films have higher absorption coefficients at longer wavelengths compared to relaxed films. Figure 3(a) also shows that the absorption of the Ge slab with 0.2% strain has higher absorption toward longer wavelengths compared to the one without any strain (black versus blue lines). However, the overall EQE enhancement in PDs without holes is not significant by introducing only 0.2% strain in the Ge layer. On the other hand, the 0.2% strain in the Ge PDs with holes does not affect the EQE/absorption much compared to that without strain (red versus green lines). Either case shows significant enhancement on the EQE compared to the case without holes, which proves the effectiveness of the photon-trapping holes. A Ge-on-Si PD with an EQE independent of strain level to some extent can promote the reliability of optical receivers made of Ge PDs.

Figure 3(b) shows transmission and reflection spectra simulated for the PDs with (red lines) and without (black lines) holes. For shorter wavelengths, the periodic holes suppress the surface reflection, as the reflection spectrum suggests, and thus result in a higher absorption. For longer wavelengths, light is trapped in the structure with holes as the transmission spectrum suggests. Therefore, absorption enhancement at the longer wavelengths is predominantly determined by light-guiding enabled by the periodic hole arrays. Figure 3(b) also compares the cases for a strained and a relaxed Ge layer. The transmission spectrum for PDs with holes indicates almost no difference for the cases of strained and relaxed Ge, suggesting the effective mechanism is light trapping in PDs with hole arrays. A slight difference in the absorption spectrum of PDs with holes toward longer wavelengths can be attributed to lower reflection of light with a strained Ge layer, as indicated by Fig. 3(b) inset. In the case of PDs without holes, reflection spectra for strained and relaxed Ge resemble each other, and the slightly improved EQE with strain is due mostly to the shift in transmission spectrum toward longer wavelengths.

3. DEVICE STRUCTURE AND FABRICATION

The pin layers of Ge photodiodes were epitaxially grown on an Si substrate. A 2 μm thick intrinsic Ge layer is sandwiched between a highly phosphorus doped (10^{19} cm^{-3}) Si n-type contact layer and a highly boron doped (10^{20} cm^{-3}) Ge p-type layer (both contact layers are designed to be 0.2 μm thick), as shown in Fig. 1. The contact layers are highly doped to reduce the minority carriers' lifetime outside the space charge region and minimize their diffusion. The intrinsic Ge layer is kept relatively thin to be able to minimize the transit time of photogenerated electrons and holes, thus making the PD operate at a high speed.

All the fabrication processes for the Ge photodiodes are CMOS compatible and were conducted in a class 100 cleanroom. The as-grown Ge-on-Si wafer was first cleaned in PRS3000 solution to remove any organic contaminant. Then, 0.9 μm i-line resist was uniformly spin-coated onto the Ge-on-Si wafer. GCA 8500 i-line stepper was used as the exposure tool to pattern the i-line resist. Similar to the reactive ion etch (RIE) technique performed on silicon described in Refs. [28,29], funnel-shaped microholes were created on the Ge surface, as Fig. 4 shows. Briefly, the resist between the dense holes can form

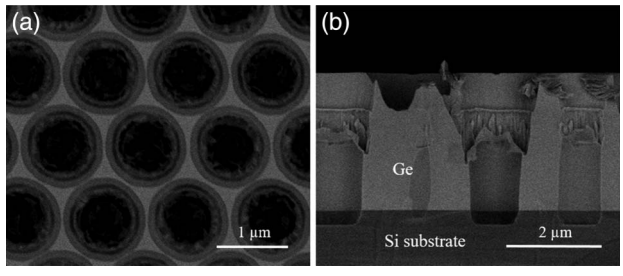

Fig. 4. (a) Top view scanning electron microscope (SEM) image of funnel-shaped holes on the Ge surface. The holes are 1.1 μm in diameter and 1.2 μm in period, and in a hexagonal lattice. (b) Cross-sectional SEM image of the funneled holes showing sidewall angle of around 65°. The Ge and Si interface is also clearly shown in this image.

positive angles due to the lateral etch of the resist in RIE. After a critical thickness of the resist (~200 nm) is reached, the microholes in Ge start to widen and form a tapered angle. The resist thickness has to be calibrated by taking into consideration of the etch ratio of the Ge and resist, so that the desired depth of the holes can be reached. As also described in Refs. [28,29], compared to straight holes, the funnel-shaped microholes with some degree of tapering angle can reduce the reflection, and thus improve the quantum efficiency of the PDs. After the holes etch, the PD mesa structures were etched to the respective layers via RIE: p-mesa was etched through the p+Ge and i-Ge layers and stopped at the n+Si layer, and n-mesa was etched through the n+Si layer and stopped at the Si substrate. 10 nm of SiO_2 was then deposited using plasma enhanced atomic layer deposition (ALD) at 270°C as a device passivation layer to minimize the dark current [34]. Metal layer stacks composed of 100 nm Al, 10 nm Ti, and 30 nm Pt were deposited sequentially on p-mesa and n-mesa by sputtering, followed by a lift-off process. Ohmic contacts between the metal and semiconductors were formed by rapid thermal processing (RTP) at 465°C for 30 s in a forming gas (H_2/N_2) environment. Next, an additional layer of polyimide (3 μm thick) was used for planarization as well as reducing the parasitic capacitance of coplanar waveguides (CPWs). Last, CPWs composed of 10 nm Ti and 300 nm Al were sputtered followed by a lift-off process.

4. RESULTS AND DISCUSSION

A. Strains in the Ge Epi Film

In our design, n-type Si epi layer was first grown on the Si substrate at 950°C via epitaxial chemical vapor deposition. The heteroepitaxy of Ge on Si was initialized by a low-temperature deposited Ge seed layer at 400°C to minimize the dislocation densities at the Ge/Si interfaces [22,23]. Then, the growth temperature was raised to 700°C to grow the intrinsic and p-type Ge epi layers. Because of the different CTEs between Ge and Si substrate, a tensile strain can be formed in the Ge film upon cooling from the growth temperature to room temperature [20,35,36]. The strain states in our Ge layers were characterized by high-resolution XRD (HRXRD). Figure 5 depicts the HRXRD (004) $\theta - 2\theta$ scan of the pin Ge epi layers on Si substrate as compared to the bulk Ge as a reference. The XRD peak for Ge shifts from 65.994° to 66.12°. Using the relationship and calculation of the lateral and vertical lattice constant described in Ref. [37], the strain in our Ge film is estimated to be 0.23%, which is close to the values reported in previous studies [34,38,39] using similar growth conditions.

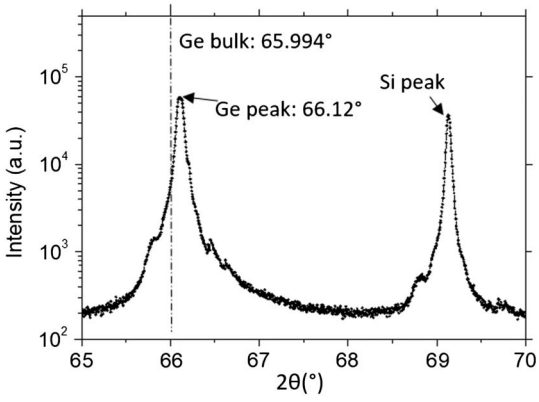

Fig. 5. HRXRD (004) $\theta - 2\theta$ scan of Ge epi layers on Si substrate. The dashed line represents the peak of bulk Ge as a reference.

B. Improved EQE of Ge PDs by Photon-Trapping Holes

EQE, defined as the ratio of the number of charge carriers generated by incoming light to the number of incident photons, is an important metric to determine how sensitive a PD is. Measurements of EQE in Ge on Si PDs are performed using an NKT supercontinuum laser and a tunable filter that allows transmission of individual wavelengths with 5 nm resolution. A single-mode optical fiber was used to deliver the light to the PDs, and a semiconductor parameter analyzer (Agilent 4155B) was used to apply the electrical potential and measure the output current of the PDs. Dark current measurement was also performed under a no light illumination condition using the same setup. The EQEs of Ge-on-Si PDs with funnel-shaped photon-trapping holes (diameter, 1150 nm; period, 1750 nm; hexagonal lattice) were measured between the wavelengths of 1200 and 1800 nm. In addition, PDs without holes were also characterized for comparison. Figure 6(a) represents the measured EQEs at 1550 nm wavelength from various hole designs. It should be noted that the PDs with larger holes seem to have better EQEs at the wavelength of 1550 nm, which is different from our previous work on Si PDs at 800–980 nm wavelengths, where smaller holes outperform [28,29]. As for Ge PDs, the target wavelength is longer, and the diameter and period of the holes should also be large enough to couple lateral modes into the device structure. Since holes with diameter/period of 1150/1750 nm in a hexagonal lattice showed the best EQE at 1550 nm, we used these hole arrays as the optimum design for our Ge PDs, and further characterization was based on this design.

Figure 6(b) shows the measured EQEs and absorption in the i-layer calculated by FDTD simulations in a wavelength range of 1200 to 1800 nm. After a set of iterations, it was found that the absorption simulated by assuming a 1.1 μm thick effective i-layer fits well with the experimental results. The gradual change in doping profiles at both boundaries of the i-layer adjacent to the highly doped contact layers can lead to reduced thickness of the i-layer. Undesired dopant diffusion to the i-layer from the highly doped region during epi-growth can prevent complete depletion of i-layer and cause soft regions where the applied electric field is not strong enough to collect all the carriers. Experimental and simulation results showed reasonably good agreement for the PDs with and without holes, except for the longer wavelengths beyond 1600 nm. Such discrepancy can be attributed to fabrication-related deviation and recombination loss of photo-generated carriers. Additionally, light with longer wavelengths can penetrate deep into the material and can be absorbed beyond the i-layer, where the electric field is weak for efficient carrier collection.

The enhancement in the EQEs of the Ge-on-Si PDs with photon-trapping holes is noticeable in both data communication wavelengths (1300 and 1550 nm). An 80% EQE is

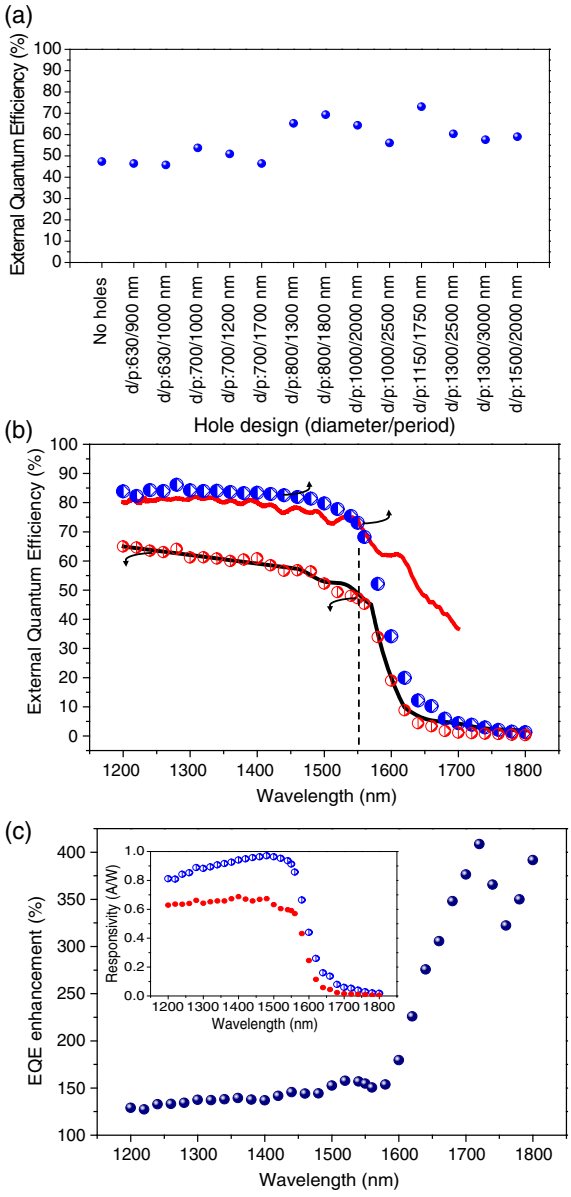

Fig. 6. (a) Measured EQEs of Ge-on-Si PDs with various designs of hole arrays at 1550 nm wavelength. The PD with hole arrays with diameter/period (d/p) of 1150/1750 nm in a hexagonal lattice has the best EQE. (b) Measured EQE versus calculated absorption of Ge-on-Si PDs with hole arrays (diameter/period: 1150/1750 nm) and without holes, for s wavelength range of 1200–1800 nm. Blue half-filled circles show measured EQE data of Ge-on-Si PDs with holes, while red half-filled circles represent measured EQEs of Ge-on-Si PD without holes. 73% EQE is recorded at 1550 nm wavelength with light-guiding holes, whereas the EQE of a PD without holes is only 47%. Red and black solid lines show the calculated absorption in PDs with and without holes, assuming 0.2% strained Ge on Si, respectively. Simulation results are in good agreement for PDs without holes, whereas PDs with holes are expected to show higher EQE at the longer wavelengths beyond 1600 nm. Such discrepancy can be attributed to the deviation in fabricated structures from design and recombination loss of photo-generated carriers. (c) Responsivity of Ge-on-Si PDs with and without holes for the wavelength range of 1200–1800 nm. 0.91 A/W responsivity is achieved at 1550 nm with holes. Inset: EQE enhancement by micro-/nanoholes, showing >350% increase in EQE with holes for wavelengths beyond 1600 nm.

achieved at 1300 nm wavelength, whereas a PD without holes provides 65% EQE. A similar trend is observed at a wavelength of 1550 nm, where the EQE is improved from 43% to 73% by photon-trapping holes. Moreover, the enhancement in EQE is present over the entire broadband of wavelengths. As shown in Fig. 6(c), it becomes more considerable at wavelengths above 1600 nm, where the EQE of Ge-on-Si PD with photon-trapping holes has 34% efficiency, whereas a Ge-on-Si PD without holes has only 19% EQE. A >350% enhancement in EQE was observed in PDs with hole arrays compared to the PDs without holes up to 1700 nm wavelength, potentially offering data transmission possible beyond the L band.

Another important figure of merit in PDs is responsivity, defined as the output electrical current of the PD produced in response to incident optical power. The inset in Fig. 6(c) shows that Ge-on-Si PDs with photon-trapping holes have achieved responsivity of 0.91 A/W at 1550 nm, whereas PDs without this photon-trapping mechanism present 0.6 A/W, representing an ~50% improvement in responsivity.

C. Electrical Characterization

1. Dark Current Density

Since the photon-trapping holes are created by dry etching with physical bombardment of high-energy plasma ions, crystalline defects and dangling bonds can be formed at the Ge surface and create surface states that can contribute to increased dark current level, and thus need to be efficiently passivated. In this work, 10 nm SiO_2 was uniformly deposited on the wafer via ALD after the hole and mesa etches for passivation. Figure 7(a) shows the dark current density (DCD)-voltage characteristics of the Ge-on-Si PDs without holes. It can be seen that at −1 V, the DCDs of PDs with different mesa diameters are between 10 and 20 mA/cm^2. These values are comparable or lower than previously reported ones [34,39–42] at reverse bias of 1 V. The

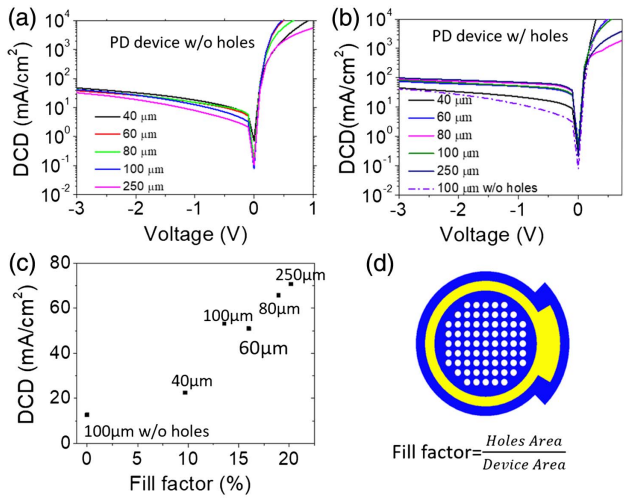

Fig. 7. (a) DCD of Ge PD devices of different mesa diameters without photon-trapping holes from −3 to 1 V. (b) DCD of Ge PD devices of different mesa diameters with photon-trapping holes (1300 nm in diameter, and 2300 nm in period) from −3 to 1 V (the dashed line shows the comparison with a 100 μm Ge PD without holes). (c) DCD of the PDs with different mesa sizes with different fill factors. (d) Schematic showing the definition of the fill factor in the PDs.

lines are all very close to each other, showing independence of the dark current level from mesa diameter. This implies effective ALD passivation on the mesa sidewall etched by RIE. As Fig. 7(b) shows, the DCD of Ge PDs with holes (1300 nm in diameter and 2300 nm in period) increased by around 3 times to 50–70 mA/cm^2 at −1 V. Only the PD with 40 μm mesa diameter has relatively small DCD of 22.5 mA/cm^2 at −1 V. Although the hole diameter and period are the same among those mesas with different sizes, the air-hole fill factors are rather different. Figure 7(c) shows the DCDs of the PD devices of different mesa sizes with the same type of holes (diameter, 1300 nm; period, 2300 nm; hexagonal lattice). Although the dimensions of the holes are the same, the air-hole fill factors are different among the PDs with different mesa sizes since the ohmic metal ring also takes up the space of the total device area [as shown in the schematic in Fig. 7(d)]. Thus, the number of holes per unit area is different in different mesa sizes. We count the total number of holes in each mesa size and then calculate the fill factor for each PD mesa size. It can be seen from Fig. 7(c) that, with larger fill factor, the DCD of the PD tends to be larger. It can be concluded that the DCD is still dependent on the total etched surface, since ALD may still leave some unpassivated surface states.

It should also be noted that the etched surface of a 100 μm device without holes is estimated to be around 785 μm^2, while the etched surface of the same size device with holes is estimated to be 10,100 μm^2, around a 13 times increase in the etched surface area. Compared to the increased etched surface, the increase in the DCD is much smaller, suggesting still reasonably good passivation of ALD on the sidewall of the holes. However, because of the complex geometry and surface roughness of the tapered sidewall in the holes created by the dry etch, the ALD SiO_2 layer may still leave some unpassivated surface states, which ultimately contribute to the increase in the DCD.

2. High Speed

Ge-on-Si PDs were surface illuminated with a fiber probe that is connected to a fiber-coupled continuum laser filtered at 1300 nm. The optical pulse width was ~15 ps at this wavelength. The electrical pulses, because of the photoresponse of the PD, were collected by a 20 GHz sampling scope. The PD under test was DC biased using a 25 GHz bias-T.

Figure 8 shows the resultant pulse response (blue circles) measured from a photon-trapping PD with a mesa diameter of 30 μm. A PD without holes was also tested under the same conditions as a comparison. An improvement in the FWHM of the pulse response was observed with the PD with photon-trapping holes compared to the one without holes. The FWHM of the pulse response of PD with hole arrays is 75 ps, whereas the FWHM is 80 ps in the case of the PD without holes. However, the actual response of the device can be estimated by considering the response of the scope and the laser source using the following equation [43]:

$$\tau_{\text{means}} = \sqrt{\tau_{\text{actual}}^2 + \tau_{\text{scope}}^2 + \tau_{\text{optical}}^2},$$

where τ_{means}, τ_{actual}, τ_{scope}, and τ_{optical} are the measured, actual, oscilloscope, and laser optical pulse widths in the time domain. The actual responses of the PDs with and without holes were

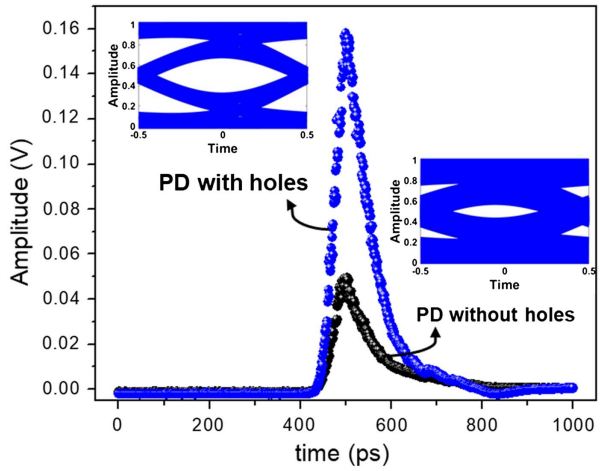

Fig. 8. High-speed responses of a 30 μm PD with (blue) and without (black) holes, observed by a 20 GHz oscilloscope after illuminating the PD with a sub-picosecond optical pulse at 1300 nm wavelength. The insets show the simulated eye diagrams at the filter output for 10 Gb/s data transmission rate for PDs with and without holes.

estimated as 70 and 76 ps, respectively, by considering a 20 ps FWHM response for the 20 GHz sampling scope and the optical laser pulse width of ~15 ps.

A diffusion tail was observed after the pulse fall-time due to the slow carriers generated in the transition regions (p-i and i-n boundary regions). The dopant diffusion during epitaxial growth made the transition regions longer and softer where the applied field is not strong enough to drift the photogenerated carriers. This diffusion tail also verifies our hypothesis on the reduction of the effective i-layer in the FDTD simulation in Section 2.

Another advantage of holes is to reduce the junction capacitance by decreasing the junction area [44]. That helps to reduce RC time, which is one of the factors limiting the speed of a pin diode. The capacitance reduction in our Ge-on-Si PDs with holes results in faster response compared to its counterpart without holes.

A computer simulation is used to evaluate the performance of Ge PDs with and without hole arrays for transmission speed. A pattern consisting of 2000 random bits was convolved with the PD impulse responses. The effect of a trans-impedance amplifier (TIA) was included in the simulations by applying the PD output to a third-order Butterworth filter with a 3 dB bandwidth equal to 0.75× bit rate [45,46]. The insets in Fig. 8 show the simulated eye diagrams at the filter output for a 10 Gb/s data transmission rate, indicating possible operation at such a rate. Compared to the eye diagrams generated with the measured impulse response of Ge PDs without hole arrays, there is an apparent improvement in transmission speed by Ge PDs with hole arrays, securing 10 Gb/s operation.

5. CONCLUSIONS

A surface-illuminated Ge-on-Si photodiode with photon-trapping holes has been demonstrated in this work. The photon-trapping holes have enabled lateral propagation modes in the thin Ge layers and, thus, successfully improved the

external quantum efficiencies of the PDs at wavelengths between 1200 and 1800 nm. EQEs of 80% and 73% (responsivity of 0.91 A/W) have been demonstrated at two data communication wavelengths (1300 and 1550 nm), respectively, both showing enhancement compared to Ge-on-Si PDs without holes. In addition, more than 3.5-fold increase in EQEs has been achieved at longer wavelengths beyond the L band (1620 nm), which makes these PDs attractive for a new data transmission window. The photon-trapping holes also reduce the temporal response of the PDs by reducing the junction capacitance. The Ge-on-Si PD with photon-trapping holes has an FWHM temporal response of 70 ps, which is suitable for 10 Gb/s data transmission operation. Our Ge-on-Si PDs with 2D arrays of high-density photon-trapping holes have the potential to be monolithically integrated with CMOS/BiCMOS ASICs. Such monolithic integration offers low-cost packaging solutions and allows low parasitics, resulting in high performance. Ge-on-Si PDs with photon-trapping holes can have applications for short- and long-reach communication at intra- and inter-datacenters, passive optical networks [3], lidar [47,48], and quantum communication systems [49], as well as enhancing the capacity of long-haul DWDM systems beyond the L band. Our future work will focus on optimization of the dopant diffusion between the highly doped and intrinsic regions of pin PDs to avoid a diffusion tail in the temporal response.

Funding. Army Research Office (ARO) (W911NF-14-4-0341); W&WSens Devices, Inc.

Acknowledgment. The authors thank S. P. Wang and S. Y. Wang partnership for the financial support.

†These authors contributed equally to this work.

REFERENCES

1. O. Vermesan and P. Friess, *Internet of Things: Converging Technologies for Smart Environments and Integrated Ecosystems* (River, 2013).
2. Y. A. Vlasov, "Silicon CMOS-integrated nano-photonics for computer and data communications beyond 100G," IEEE Commun. Mag. **50**, s67–s72 (2012).
3. V. Houtsma, D. van Veen, and E. Harstead, "Recent progress on standardization of next-generation 25, 50, and 100G EPON," J. Lightwave Technol. **35**, 1228–1234 (2017).
4. Z. Li, Y.-M. Jung, N. Simakov, P. Shardlow, A. Heidt, A. Clarkson, S.-U. Alam, and D. J. Richardson, "Extreme short wavelength operation (1.65–1.7 μm) of silica-based thulium-doped fiber amplifier," in *Optical Fiber Communication Conference* (Optical Society of America, 2015), paper Tu2C.1.
5. S. V. Firstov, S. V. Alyshev, K. E. Riumkin, V. F. Khopin, A. N. Guryanov, M. A. Melkumov, and E. M. Dianov, "A 23-dB bismuth-doped optical fiber amplifier for a 1700-nm band," Sci. Rep. **6**, 28939 (2016).
6. H. Zhang, Z. Li, N. Kavanagh, J. Zhao, N. Ye, Y. Chen, N. Wheeler, J. Wooler, J. Hayes, and S. Sandoghchi, "81 Gb/s WDM transmission at 2 μm over 1.15 km of low-loss hollow core photonic bandgap fiber," in *European Conference on Optical Communication (ECOC)* (IEEE, 2014).
7. T. Morioka, Y. Awaji, R. Ryf, P. Winzer, D. Richardson, and F. Poletti, "Enhancing optical communications with brand new fibers," IEEE Commun. Mag. **50**, s31–s42 (2012).
8. P. Jouguet, S. Kunz-Jacques, A. Leverrier, P. Grangier, and E. Diamanti, "Experimental demonstration of long-distance continuous-variable quantum key distribution," Nat. Photonics **7**, 378–381 (2013).
9. R. Sabatini, M. A. Richardson, H. Jia, and D. Zammit-Mangion, "Airborne laser systems for atmospheric sounding in the near infrared," Proc. SPIE **8433**, 843314 (2012).
10. L. A. Sordillo, Y. Pu, S. Pratavieira, Y. Budansky, and R. R. Alfano, "Deep optical imaging of tissue using the second and third near-infrared spectral windows," J. Biomed. Opt. **19**, 056004 (2014).
11. S. Gunapala, B. Levine, D. Ritter, R. Hamm, and M. Panish, "InGaAs/InP long wavelength quantum well infrared photodetectors," Appl. Phys. Lett. **58**, 2024–2026 (1991).
12. H. Ito, T. Furuta, S. Kodama, and T. Ishibashi, "InP/InGaAs uni-travelling-carrier photodiode with 310 GHz bandwidth," Electron. Lett. **36**, 1809–1810 (2000).
13. H. Cansizoglu, E. P. Devine, Y. Gao, S. Ghandiparsi, T. Yamada, A. F. Elrefaie, S.-Y. Wang, and M. S. Islam, "A new paradigm in high-speed and high-efficiency silicon photodiodes for communication—Part I: enhancing photon-material interactions via low-dimensional structures," IEEE Trans. Electron Devices **65**, 372–381 (2018).
14. H. Cansizoglu, A. F. Elrefaie, C. Bartolo-Perez, T. Yamada, Y. Gao, A. S. Mayet, M. F. Cansizoglu, E. P. Devine, S.-Y. Wang, and M. S. Islam, "A new paradigm in high-speed and high-efficiency silicon photodiodes for communication—Part II: device and VLSI integration challenges for low-dimensional structures," IEEE Trans. Electron Devices **65**, 382–391 (2018).
15. J. S. Dunn, D. C. Ahlgren, D. D. Coolbaugh, N. B. Feilchenfeld, G. Freeman, D. R. Greenberg, R. A. Groves, F. J. Guarin, Y. Hammad, A. J. Joseph, L. D. Lanzerotti, S. A. St. Onge, B. A. Orner, J.-S. Rieh, K. J. Stein, S. H. Voldman, P.-C. Wang, M. J. Zierak, S. Subbanna, D. L. Harame, D. A. Herman, and B. S. Meyerson, Jr., "Foundation of RF CMOS and SiGe BiCMOS technologies," IBM J. Res. Dev. **47**, 101–138 (2003).
16. S. Sze, *Physics of Semiconductor Devices* (Wiley, 1981).
17. H. Ye and J. Yu, "Germanium epitaxy on silicon," Sci. Technol. Adv. Mater. **15**, 024601 (2014).
18. J. Michel, J. Liu, and L. C. Kimerling, "High-performance Ge-on-Si photodetectors," Nat. Photonics **4**, 527–534 (2010).
19. A. Beling and J. C. Campbell, "High-speed photodiodes," IEEE J. Sel. Top. Quantum Electron. **20**, 57–63 (2014).
20. A. N. Larsen, "Epitaxial growth of Ge and SiGe on Si substrates," Mater. Sci. Semicond. Process. **9**, 454–459 (2006).
21. Z. Huang, J. Oh, and J. C. Campbell, "Back-side-illuminated high-speed Ge photodetector fabricated on Si substrate using thin SiGe buffer layers," Appl. Phys. Lett. **85**, 3286–3288 (2004).
22. L. Colace, G. Masini, F. Galluzzi, G. Assanto, G. Capellini, L. Di Gaspare, E. Palange, and F. Evangelisti, "Metal-semiconductor–metal near-infrared light detector based on epitaxial Ge/Si," Appl. Phys. Lett. **72**, 3175–3177 (1998).
23. H.-C. Luan, D. R. Lim, K. K. Lee, K. M. Chen, J. G. Sandland, K. Wada, and L. C. Kimerling, "High-quality Ge epilayers on Si with low threading-dislocation densities," Appl. Phys. Lett. **75**, 2909–2911 (1999).
24. H.-Y. Yu, J.-H. Park, A. K. Okyay, and K. C. Saraswat, "Selective-area high-quality germanium growth for monolithic integrated optoelectronics," IEEE Electron Device Lett. **33**, 579–581 (2012).
25. D. Houghton, "Strain relaxation kinetics in $Si_{1-x}Ge_x$/Si heterostructures," J. Appl. Phys. **70**, 2136–2151 (1991).
26. F. LeGoues, B. Meyerson, and J. Morar, "Anomalous strain relaxation in SiGe thin films and superlattices," Phys. Rev. Lett. **66**, 2903–2906 (1991).
27. O. I. Dosunmu, D. D. Cannon, M. K. Emsley, L. C. Kimerling, and M. S. Unlu, "High-speed resonant cavity enhanced Ge photodetectors on reflecting Si substrates for 1550-nm operation," IEEE Photon. Technol. Lett. **17**, 175–177 (2005).
28. Y. Gao, H. Cansizoglu, K. G. Polat, S. Ghandiparsi, A. Kaya, H. H. Mamtaz, A. S. Mayet, Y. Wang, X. Zhang, T. Yamada, E. P. Devine, A. F. Elrefaie, S.-Y. Wang, and M. S. Islam, "Photon-trapping microstructures enable high-speed high-efficiency silicon photodiodes," Nat. Photonics **11**, 301–308 (2017).

29. Y. Gao, H. Cansizoglu, S. Ghandiparsi, C. Bartolo-Perez, E. P. Devine, T. Yamada, A. F. Elrefaie, S.-Y. Wang, and M. S. Islam, "High speed surface illuminated Si photodiode using microstructured holes for absorption enhancements at 900–1000 nm wavelength," ACS Photon. **4**, 2053–2060 (2017).
30. S. Peng and G. M. Morris, "Resonant scattering from two-dimensional gratings," J. Opt. Soc. Am. A **13**, 993–1005 (1996).
31. Q. C. Nie and B. K. Chen, "Application of ADE-FDTD method in lossy Lorentz media," in *Advanced Materials Research* (Trans Tech, 2014), pp. 2486–2489.
32. H. Wen and E. Bellotti, "Rigorous theory of the radiative and gain characteristics of silicon and germanium lasing media," Phys. Rev. B **91**, 035307 (2015).
33. M. J. Süess, R. Geiger, R. Minamisawa, G. Schiefler, J. Frigerio, D. Chrastina, G. Isella, R. Spolenak, J. Faist, and H. Sigg, "Analysis of enhanced light emission from highly strained germanium microbridges," Nat. Photonics **7**, 466–472 (2013).
34. Y. Lin, K. H. Lee, S. Bao, X. Guo, H. Wang, J. Michel, and C. S. Tan, "High-efficiency normal-incidence vertical p-i-n photodetectors on a germanium-on-insulator platform," Photon. Res. **5**, 702–709 (2017).
35. J. Liu, D. D. Cannon, K. Wada, Y. Ishikawa, S. Jongthammanurak, D. T. Danielson, J. Michel, and L. C. Kimerling, "Tensile strained Ge p-i-n photodetectors on Si platform for C and L band telecommunications," Appl. Phys. Lett. **87**, 011110 (2005).
36. J. Liu, R. Camacho-Aguilera, J. T. Bessette, X. Sun, X. Wang, Y. Cai, L. C. Kimerling, and J. Michel, "Ge-on-Si optoelectronics," Thin Solid Films **520**, 3354–3360 (2012).
37. J. M. Hartmann, A. Abbadie, A. M. Papon, P. Holliger, G. Rolland, T. Billon, J. M. Fédéli, M. Rouvière, L. Vivien, and S. Laval, "Reduced pressure-chemical vapor deposition of Ge thick layers on Si(001) for 1.3–1.55-μm photodetection," J. Appl. Phys. **95**, 5905–5913 (2004).
38. L. Colace, M. Balbi, G. Masini, G. Assanto, H.-C. Luan, and L. C. Kimerling, "Ge on Si p-i-n photodiodes operating at 10 Gbit/s," Appl. Phys. Lett. **88**, 101111 (2006).
39. D. Su, S. Kim, J. Joo, and G. Kim, "36-GHz high-responsivity Ge photodetectors grown by RPCVD," IEEE Photon. Technol. Lett. **21**, 672–674 (2009).
40. L. Colace, G. Masini, G. Assanto, H.-C. Luan, K. Wada, and L. Kimerling, "Efficient high-speed near-infrared Ge photodetectors integrated on Si substrates," Appl. Phys. Lett. **76**, 1231–1233 (2000).
41. C. Li, C. Xue, Z. Liu, B. Cheng, C. Li, and Q. Wang, "High-bandwidth and high-responsivity top-illuminated germanium photodiodes for optical interconnection," IEEE Trans. Electron Devices **60**, 1183–1187 (2013).
42. Z. Zhou, J. He, R. Wang, C. Li, and J. Yu, "Normal incidence p-i-n Ge heterojunction photodiodes on Si substrate grown by ultrahigh vacuum chemical vapor deposition," Opt. Commun. **283**, 3404–3407 (2010).
43. K. Rush, S. Draving, and J. Kerley, "Characterizing high-speed oscilloscopes," IEEE Spectr. **27**, 38–39 (1990).
44. H. Cansizoglu, Y. Gao, S. Ghandiparsi, A. Kaya, C. B. Perez, A. Mayet, E. P. Devine, M. F. Cansizoglu, T. Yamada, and A. F. Elrefaie, "Improved bandwidth and quantum efficiency in silicon photodiodes using photon-manipulating micro/nanostructures operating in the range of 700–1060 nm," Proc. SPIE **10349**, 103490U (2017).
45. B. Moeneclaey, G. Kanakis, J. Verbrugghe, N. Iliadis, W. Soenen, D. Kalavrouziotis, C. Spatharakis, S. Dris, X. Yin, and P. Bakopoulos, "A 64 Gb/s PAM-4 linear optical receiver," in *Optical Fiber Communication Conference* (Optical Society of America, 2015), paper M3C.5.
46. D. Okamoto, Y. Suzuki, K. Yashiki, Y. Hagihara, M. Tokushima, J. Fujikata, M. Kurihara, J. Tsuchida, T. Nedachi, and J. Inasaka, "A 25-Gb/s 5 × 5 mm 2 chip-scale silicon-photonic receiver integrated with 28-nm CMOS transimpedance amplifier," J. Lightwave Technol. **34**, 2988–2995 (2016).
47. A. McCarthy, X. Ren, A. Della Frera, N. R. Gemmell, N. J. Krichel, C. Scarcella, A. Ruggeri, A. Tosi, and G. S. Buller, "Kilometer-range depth imaging at 1550 nm wavelength using an InGaAs/InP single-photon avalanche diode detector," Opt. Express **21**, 22098–22113 (2013).
48. M. Ren, X. Gu, Y. Liang, W. Kong, E. Wu, G. Wu, and H. Zeng, "Laser ranging at 1550 nm with 1-GHz sine-wave gated InGaAs/InP APD single-photon detector," Opt. Express **19**, 13497–13502 (2011).
49. R. H. Hadfield, "Single-photon detectors for optical quantum information applications," Nat. Photonics **3**, 696–705 (2009).